Discovery of highly spin-polarized conducting surface states in the strong spin-orbit coupling semiconductor Sb_2Se_3

Shekhar Das,[1] Anshu Sirohi,[1] Gaurav Kumar Gupta,[2] Suman Kamboj,[1] Aastha Vasdev,[1] Sirshendu Gayen,[1] Prasenjit Guptasarma,[3] Tanmoy Das,[2] and Goutam Sheet[1,*]

[1]*Department of Physical Sciences, Indian Institute of Science Education and Research Mohali, Sector 81, S. A. S. Nagar, Manauli, P.O. Box 140306, India*

[2]*Department of Physics, Indian Institute of Science, Bangalore 560012, India*

[3]*Department of Physics, University of Wisconsin, Milwaukee, Wisconsin 53211, USA*

(Received 4 January 2018; published 8 June 2018)

Majority of the A_2B_3-type chalcogenide systems with strong spin-orbit coupling (SOC), such as Bi_2Se_3, Bi_2Te_3, and Sb_2Te_3, etc., are topological insulators. One important exception is Sb_2Se_3 where a topological nontrivial phase was argued to be possible under ambient conditions, but such a phase could be detected to exist only under pressure. In this paper, we show that Sb_2Se_3 like Bi_2Se_3 displays a generation of highly spin-polarized current under mesoscopic superconducting point contacts as measured by point-contact Andreev reflection spectroscopy. In addition, we observe a large negative and anisotropic magnetoresistance of the mesoscopic metallic point contacts formed on Sb_2Se_3. Our band-structure calculations confirm the trivial nature of Sb_2Se_3 crystals and reveal two trivial surface states one of which shows large spin splitting due to Rashba-type SOC. The observed high spin polarization and related phenomena in Sb_2Se_3 can be attributed to this spin splitting.

DOI: 10.1103/PhysRevB.97.235306

Within the band theory of solids metals and insulators are distinguished based on a band gap which is either zero for metals or nonzero for insulators. A topological insulator behaves like an insulator with a band gap in the bulk, but the surface contains gapless conducting states protected by time-reversal symmetry [1–4]. In such systems strong spin-orbit coupling acts as an effective magnetic field pointing in a spin-dependent direction thereby giving rise to nonzero spin polarization of the conducting surface states [5–7]. In other words, the charge carriers corresponding to these surface states have the spin angular momentum locked with the orbital angular momentum which means carriers with definite momentum direction have definite spin. The spin polarization of the surface states of topological insulators were measured in the past by a number of techniques. The most widely exploited techniques included spin-resolved angle-resolved photoemission spectroscopy [8–10] and using circularly polarized photons to excite the spin-polarized photocurrent [11–13]. Electrical methods based on fabrication of devices involving topological insulators have also been employed [14,15]. More recently it was shown that point-contact Andreev reflection (PCAR) spectroscopy using a sharp tip of a conventional superconductor on the surface of a topological insulator can also be used to measure the spin polarization of the surface states through the measurement of the degree of suppression of Andreev reflection [16].

Andreev reflection at an interface between a conventional superconductor and a topological material should be analyzed carefully as coupling between the superconducting order and the topological phase may be complex, particularly because of the possibility of the emergence of a topological superconductor at such interfaces [17–22]. This aspect was studied in the past, and it was found that the proximity-induced superconductivity in point-contact geometries on topological insulators has a far greater nontopological character than topological [23]. From Andreev reflection experiments on various topological insulators it was found that spin polarization in doped topological insulators can vary with the level of doping. The topological insulators Bi_2Te_3 and Sb_2Te_3 showed spin polarization of 70% and 57%, respectively [16]. In all these cases, a conventional modified Blonder-Tinkham-Klapwijk (BTK) theory was used for the analysis [24,25].

Based on earlier band-structure calculations [2,26] Sb_2Se_3, a member of the A_2B_3-type chalcogenide family with high spin-orbit coupling was categorized as a trivial band insulator under ambient conditions. Some experiments indicated the possibility of a topologically nontrivial character emerging in Sb_2Se_3 under a pressure of several gigapascals (GPas) [27–30]. More recent band-structure calculations claimed Sb_2Se_3, in fact, can be a topological insulator under ambient conditions [31]. In this paper, from spin-polarized Andreev reflection spectroscopy measurements, we show that the surface of Sb_2Se_3 contains highly spin-polarized surface states (with up to 70% spin polarization) that take part in conduction leading to the generation of highly spin-polarized current. The observations are consistent with our band-structure calculations which reveal the existence of two trivial surface states in Sb_2Se_3 one of which undergoes Rashba-type SOC-induced spin splitting.

First we confirmed the surface quality of the Sb_2Se_3 crystals using a low-temperature and ultra-high-vacuum scanning tunneling microscope (STM) working down to 300 mK. The crystals were cleaved *in situ* at 80 K under ultrahigh vacuum

*goutam@iisermohali.ac.in

 ©2018 American Physical Society

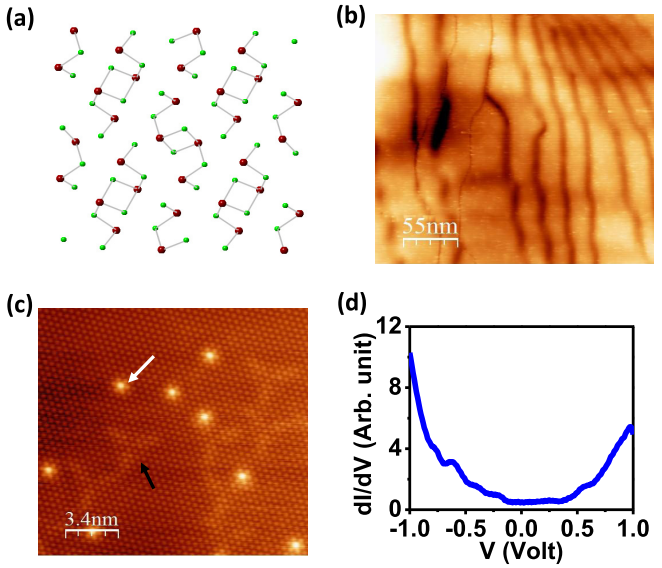

FIG. 1. (a) Crystal structure of Sb_2Se_3 viewed from the [001] direction of the crystal. (b) A large area (281 × 281 nm^2) STM topograph on Sb_2Se_3 showing atomically sharp terraces. The parameters are $T = 17$ K, $V_s = 700$ mV, and $I_s = 100$ pA. (c) A representative atomic resolution image over an area of 17 × 17 nm^2 on one of the terraces. (d) A scanning tunneling conductance spectrum recorded away from the defects.

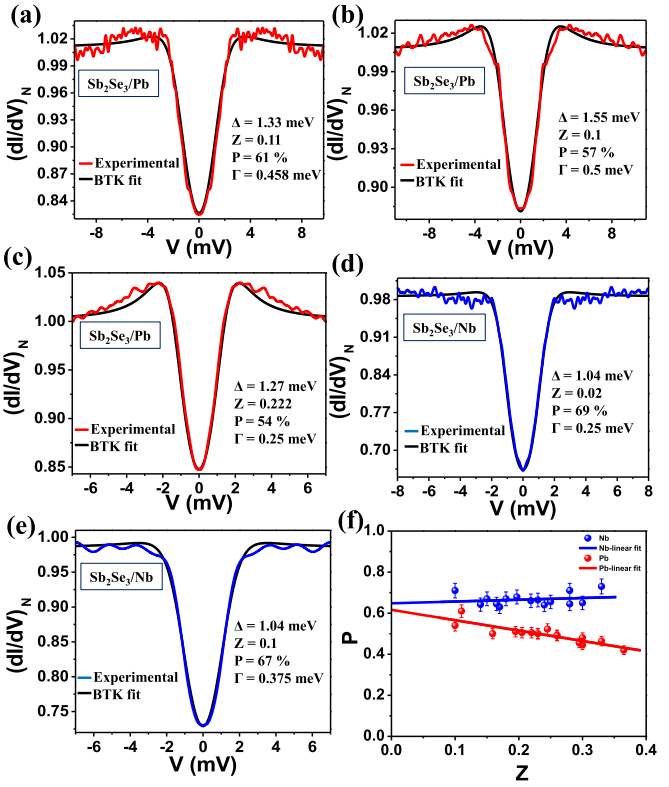

FIG. 2. Normalized dI/dV spectra for point contacts on Sb_2Se_3 with (a)–(c) Pb tips and (d) and (e) Nb tips. The black lines show BTK fits with spin polarization included. (f) Spin-polarization (P) vs barrier strength (Z) plot. The solid lines show extrapolation to $Z = 0$ where the spin polarization approaches 70%.

and were immediately transferred to the STM measurement head kept at low temperatures. A large area STM image of the Sb_2Se_3 surface shows multiple extended atomic terraces with sharp steps as shown in Fig. 1(b). Small area scans on top of the terraces and inside the trenches between two atomic terraces resolved atoms and the defect states [Fig. 1(c)]. Two types of defects are observed with one type having triangular shapes (black arrow) and the other types appear as bright spots (white arrow). The respective sides of the triangles for different triangular-shaped defects are all parallel to each other, and all such defects are randomly distributed throughout the crystal surface. The triangular defects are known to be associated with Se vacancy in the binary selenide family of materials, such as Bi_2Se_3 [32,33]. The bright spots observed here might be due to Sb defects in the crystals. In Fig. 1(d) we plot a typical local density of states (LDOS) spectrum recorded on Sb_2Se_3 away from the defects. The LDOS spectrum exhibits a "U" shape with a flat bottom indicating a gap of ∼1 eV opening with the Fermi energy falling within the gap. The LDOS within the gap region does not become absolutely zero. These low-energy states could emerge from possible surface states in Sb_2Se_3. However, no clear signature of a surface "Dirac cone" was observed which is again consistent with the nontopological nature of Sb_2Se_3.

Point-contact Andreev reflection spectroscopy measurements [34–36] on Sb_2Se_3 crystals were performed using sharp tips of two conventional superconductors Pb and Nb. In Figs. 2(a)–2(e) we show the representative Andreev reflection spectra obtained on Sb_2Se_3 with the Pb and the Nb tips, respectively. The sharp dip structure at $V = 0$ along with two shallow peaks symmetric about $V = 0$ in the normalized dI/dV spectra indicate considerable suppression of Andreev reflection. The black lines show the fit to the experimentally obtained spectra using BTK theory modified for the finite spin polarization of the nonsuperconducting electrode. The extracted values of spin-polarization P are also shown. For low values of Z, the spin polarization is measured to be almost 70%. For both Nb and Pb tips the extracted values of P are also seen to slightly depend (linearly) on Z as shown in Fig. 2(f). The solid lines in Fig. 2(f) show linear extrapolation of the Z dependence of P to $Z = 0$. This is the expected intrinsic value of the spin polarization (for $Z = 0$). The intrinsic spin polarization in this case is found to be approximately 65% which is significantly large compared to some of the strong elemental ferromagnetic metals [37], such as Fe ($P = 40\%$), Co ($P = 42\%$), and nickel ($P = 39\%$) and is comparable to the spin polarization of 70% measured by Andreev reflection spectroscopy in Bi_2Te_3 [16]. It is interesting to note that unlike in the case of Bi_2Te_3 where two gap amplitudes were considered for fitting the Andreev reflection spectra, in the case of Sb_2Se_3, only a single gap amplitude(Δ) was required which varied between 1.3 and 1.5 meV as expected for Nb point contacts on a regular metal. For Pb point contacts, Δ remained comparable to the bulk gap of Pb ∼1 meV. Thus, the analysis involved only three freely varying fitting parameters—P, Z, and Γ, the effective broadening parameter. The observation of high value of spin polarization in Sb_2Se_3 indicates that although the system is not categorized as a topologically nontrivial system, there might be trivial surface

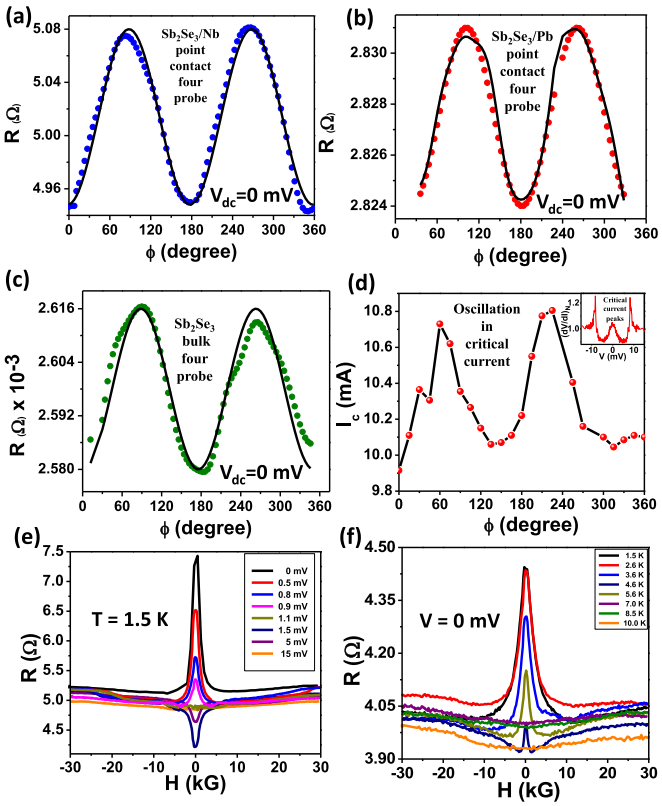

FIG. 3. Anisotropic magnetoresistance of (a) a point contact on Sb_2Se_3 with Nb. The black line shows a cos 2ϕ fit. (b) A point contact with Pb. The black line shows a cos$(2.25)\phi$ fit. (c) Bulk Sb_2Se_3 crystal. The black line shows a cos 2ϕ fit. (d) Anisotropy of the critical current of a superconducting point contact in the thermal regime. The corresponding dV/dI spectrum is shown in the *inset*. (e) Magnetoresistance of a Pb/Sb_2Se_3 point contact at different biases. $T = 1.5$ K. (f) Temperature dependence of the magnetoresistance.

states with nontrivial spin texture present due to the strong spin-orbit coupling. It should be noted that this observation is not related to the pressure-induced topological phase that was earlier observed on Sb_2Se_3 because the high spin polarization is observed even with soft tips made of superconducting Pb which cannot withstand a pressure on the order of several tens of GPa that is required to induce such a phase. Furthermore, it is known that a superconducting phase of Sb_2Se_3 is realized under high pressure [38], but we did not observe any signature of superconductivity of Sb_2Se_3.

In the context of certain other topological materials where a surface spin polarization was expected (as in the case of metallic point contacts on TaAs) [20], it was observed that the point-contact resistance showed anisotropy when the magnetic field was rotated on a plane perpendicular to the direction of the injected current. In order to investigate that possibility in Sb_2Se_3, we have performed similar experiments on the point contacts formed on Sb_2Se_3 at $V = 0$. As shown in Fig. 3(a) for point contacts with Nb and Fig. 3(b) for point contacts with Pb, the magnetoresistance of the point contacts on Sb_2Se_3 are highly anisotropic. For Nb point contacts the anisotropy is well described by a cos 2ϕ field-angle dependence, where ϕ represents the relative angle made by the magnetic-field vector with respect to the axis a on the basal plane. For Pb point contacts, the anisotropy deviated slightly from a cos 2ϕ dependence and it fitted well with cos$(2.25)\phi$. The approximate cos 2ϕ dependence observed here is similar to what was observed in the case of TaAs point contacts in the past [20]. Furthermore, a cos 2ϕ angular dependence of the anisotropic magnetoresistance is routinely observed in certain systems with large spin polarization [39] including the conventional ferromagnets [40]. Therefore, the observed field-angle dependence here further supports the existence of magnetic correlations and the occurrence of a spin-polarized transport through the point contacts on Sb_2Se_3.

It is also important to investigate whether the measured spin polarization emerges only under point contacts as seems to be the case in TaAs [41] or if that is an intrinsic surface property. In order to confirm that we measured the field-angle dependence of resistance of the crystal in a conventional four-probe geometry, the four-probe resistance is also seen to be anisotropic confirming that the anisotropic magnetoresistance is not confined to the mesoscopic point contacts but originates from magnetic correlations on the Sb_2Se_3 surface. As can be seen in Fig. 3(c), the anisotropy in magnetoresistance is 1000 times smaller than that in the point contacts but again shows a reasonably good cos 2ϕ dependence. The anisotropy of the magnetoresistance of the mesoscopic point contacts and the four-probe surface resistance can be attributed to the possible anisotropy of the effective spin-orbit coupling in Sb_2Se_3. Such anisotropy of the four-probe magnetoresistance was earlier observed in the topological insulator Bi_2Se_3 [42]. Therefore, the observed anisotropy also indicates that the highly spin-polarized surface states are indeed governed by the strong spin-orbit coupling in Sb_2Se_3.

When the superconducting electrodes are in proximity of highly spin-polarized states, the critical current of the point contacts must also be modulated by the magnetic properties of such states. For investigating the modulation of the critical current with a magnetic-field angle, we first established point contacts away from the ballistic regime such that Maxwell's contribution to the total point-contact resistance becomes significant and conductance dips [36] (peaks in dV/dI) associated with critical current become prominent. Such a spectrum is shown in the *inset* of Fig. 3(d). The position of the conductance dip provides a direct measure of the critical current. After that we rotated the magnetic field on the basal plane of the crystal and recorded the spectrum for different directions of the applied magnetic field. As shown in Fig. 3(d), the critical current also oscillates with the direction of the applied magnetic field in striking agreement with the anisotropic magnetoresistance presented in Figs. 3(a)–3(c).

In the context of the spin-polarized transport in Sb_2Se_3 single crystals, it should also be noted that the point contacts obtained in the ballistic regime of transport also show negative magnetoresistance. The negative magnetoresistance data are shown in Fig. 3(f). The black curve shows the magnetoresistance at 1.5 K. The resistance shows a peak at zero magnetic field which is suppressed by a weak magnetic field. As the temperature is increased, the zero-field peak is systematically suppressed. This effect is completely suppressed at 7 K. In order to confirm whether the magnetoresistance is due to the

superconductivity of Pb alone, the experiment was carried out at different biases applied across the tip and sample [Fig. 3(e)]. It is seen that with increasing the bias the peak at zero field gradually smears out and, surprisingly, becomes a dip at a bias of 1.5 mV. With further increasing the bias, the dip starts fading away, and the magnetoresistance disappears at a bias of 15 mV which is an order of magnitude higher than the bulk superconducting gap of Pb. This shows that the magnetoresistance is not entirely due to the superconductivity of Pb, but the Sb_2Se_3 surface also has nontrivial magnetic correlations. In fact, such negative magnetoresistance and a reversal of that with an applied gate bias was observed in the past in certain topologically nontrivial systems (and systems hosting Dirac electrons) where the reversal of magnetization was attributed to a transition from weak anti-localization-dominated transport to weak-localization-dominated transport [43,44]. Although such a possibility cannot be ruled out in our point-contact data on Sb_2Se_3, proving the existence of the same in a point-contact geometry is nontrivial and may involve measurements on nanopatterned thin flakes of the crystals with a gate bias, which is beyond the scope of this paper.

Based on the key experimental observations highlighted above, it is now imperative to understand the possibility of spin-polarized surface states by investigating the band structures of our Sb_2Se_3 crystals and the role of spin-orbit coupling. Our Sb_2Se_3 crystals have an orthorhombic structure with space-group $Pnma$. Experimentally determined lattice constants are $a = 4.0345$; $b = 11.5681$; $c = 12.7341$ Å; $\alpha = \beta = \gamma = 90^\circ$. Band-structure calculations were performed using density functional theory (DFT) within the local density approximation exchange correlation as implemented in Vienna *ab initio* simulation package [45]. Projected augmented-wave pseudopotentials are used to describe the core electron in the calculation [46]. The electronic wave function is expanded using a plane wave up to a cutoff energy of 265 eV. Brillouin-zone sampling is performed by using a $(10 \times 10 \times 10)$ Monkhorst-Pack k grid. Both atomic position and cell parameters are allowed to relax until the forces on each atom are less than 0.01 eV/Å.

Sb_2Se_3 in the typical rhombohedral structure does not have sufficient SOC strength to cause topological band inversion [2]. With sufficient van der Waals interaction, a DFT calculation however predicted that Sb_2Se_3 could become a topological insulator without any experimental verifications to date [31]. The presently studied orthorhombic phase of Sb_2Se_3 (our crystals) has higher crystal symmetry, which has the tendency to reduce the SOC strength in the bulk, and hence is even less suitable for the topological insulating phase [47]. Indeed, our DFT calculations for the bulk phase indicated no signature of band inversion with SOC. In Fig. 4 we show our computed DFT band structure without and with SOC for bulk as well as for finite-size system. Without SOC, the material is a band insulator with a gap of ∼1 eV, compare Figs. 4(a) and 4(b), much larger than the band gap of Sb_2Se_3 in the rhombohedral phase shown in Fig. 4(a). Therefore, SOC fails to switch this band ordering.

However, interestingly, we found two trivial surface states without SOC for the cleave perpendicular to the c axis [see the structure in Fig. 1(a)]. This is the cleaved plane we have probed in PCAR experiments. Among these two states, one

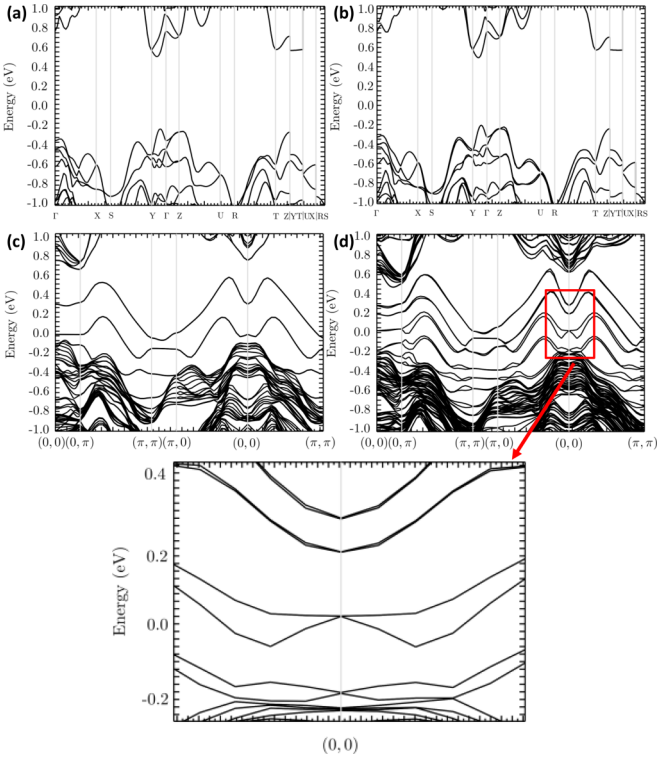

FIG. 4. Band structure of Sb_2Se_3 (a) bulk without SOC, (b) bulk with SOC, (c) for finite lattices without SOC, and (d) for finite lattices with SOC.

shows a large splitting at the surface due to Rashba-type SOC. The spin splitting is about 0.8 eV shown in Fig. 4(d), which is comparable to the experimental value. Our DFT calculations also yield a tiny magnetic phase which is however too small to open any appreciable band gap at the time-reversal invariant Γ point. Although there is a possibility that the small anisotropic field-angle dependence of magnetoresistance (Fig. 3) could originate from this tiny magnetic phase, additional experiments are required to confirm that. Therefore, DFT calculations support our observation of large spin-orbit splitting at the surface of Sb_2Se_3 which is not protected by bulk topology but with a time-reversal symmetry as in the case of a quintessential Rashba-SOC split quantum gases.

In conclusion, we have employed spin-polarized Andreev reflection spectroscopy and detected highly spin-polarized surface states in the topologically trivial band insulator Sb_2Se_3 with strong spin-orbit coupling. Furthermore, we observed highly anisotropic magnetoresistance on the basal plane of the Sb_2Se_3 crystals indicating the existence of magnetic correlations. All our experimental observations indicate that Sb_2Se_3 is a topologically trivial system. This is again consistent with our band-structure calculations which revealed the existence of trivial surface states in Sb_2Se_3 one of which undergoes spin splitting due to Rashba-type SOC thereby giving rise to the observed large value of the spin polarization and the related magnetic correlations.

We acknowledge fruitful discussions with U. Waghmare. P.G. acknowledges support from an AFOSR-MURI grant. G.S. acknowledges financial support from the research grants of (a)

a Swarnajayanti fellowship awarded by the Department of Science and Technology (DST), Government of India under Grant No. DST/SJF/PSA-01/2015-16 and (b) a research grant from DST-Nanomission under Grant No. SR/NM/NS-1249/2013.

[1] L. Fu, C. L. Kane, and E. J. Mele, Phys. Rev. Lett. **98**, 106803 (2007).
[2] H. Zhang, C.-X. Liu, X.-L. Qi, X. Dai, Z. Fang, and S.-C. Zhang, Nat. Phys. **5**, 438 (2009).
[3] B. A. Bernevig, T. L. Hughes, and S.-C. Zhang, Science **314**, 1757 (2006).
[4] L. Fu and C. L. Kane, Phys. Rev. B **76**, 045302 (2007).
[5] J. E. Moore, Nature (London) **464**, 194 (2010).
[6] C. L. Kane and E. J. Mele, Science **314**, 1692 (2009).
[7] D. Hsieh *et al.*, Science **323**, 919 (2009).
[8] D. Hsieh, Y. Xia, D. Qian, L. Wray, J. H. Dil, F. Meier, J. Osterwalder, L. Patthey, J. G. Checkelsky, N. P. Ong, A. V. Fedorov, H. Lin, A. Bansil, D. Grauer, Y. S. Hor, R. J. Cava, and M. Z. Hasan, Nature (London) **460**, 1101 (2009).
[9] S.-Y. Xu, Y. Xia, L. A. Wray, S. Jia, F. Meier, J. H. Dil, J. Osterwalder, B. Slomski, A. Bansil, H. Lin, R. J. Cava, and M. Z. Hasan, Science **332**, 560 (2011).
[10] Y. Xia, D. Qian, D. Hsieh, L Wray, A. Pal, H. Lin, A. Bansil, D. Grauer, Y. S. Hor, R. J. Cava, and M. Z. Hasan, Nat. Phys. **5**, 398 (2009).
[11] J. W. McIver, D. Hsieh, H. Steinberg, P. Jarillo-Herrero, and N. Gedik, Nat. Nanotechnol. **7**, 96 (2012).
[12] C. Jozwiak, C.-H. Park, K. Gotlieb, C. Hwang, D.-H. Lee, S. G. Louie, J. D. Denlinger, C. R. Rotundu, R. J. Birgeneau, Z. Hussain, and A. Lanzara, Nat. Phys. **9**, 293 (2013).
[13] C.-H. Park and S. G. Louie, Phys. Rev. Lett. **109**, 097601 (2012).
[14] C. H. Li, O. M. J. vant Erve, J. T. Robinson, Y. Liu, L. Li, and B. T. Jonker, Nat. Nanotechnol. **9**, 218 (2014).
[15] S. Hong, V. Diep, S. Datta, and Y. P. Chen, Phys. Rev. B **86**, 085131 (2012).
[16] K. Borisov, C.-Z. Chang, J. S. Moodera, and P. Stamenov, Phys. Rev. B **94**, 094415 (2016).
[17] P. Burset, B. Lu, G. Tkachov, Y. Tanaka, E. M. Hankiewicz, and B. Trauzettel, Phys. Rev. B **92**, 205424 (2015).
[18] Y. Kim, T. M. Philip, M. J. Park, and M. J. Gilbert, Phys. Rev. B **94**, 235434 (2016).
[19] L. Aggarwal, A. Gaurav, G. S. Thakur, Z. Haque, A. K. Ganguli, and G. Sheet, Nat. Mater. **15**, 32 (2016).
[20] L. Aggarwal, S. Gayen, S. Das, R. Kumar, V. Suess, C. Felser, C. Shekhar, and G. Sheet, Nat. Commun. **8**, 13974 (2017).
[21] L. Aggarwal, S. Gayen, S. Das, G. S. Thakur, A. K. Ganguli, and G. Sheet, Appl. Phys. Lett. **109**, 252602 (2016).
[22] S. Das, L. Aggarwal, S. Roychowdhury, M. Aslam, S. Gayen, K. Biswas, and G. Sheet, Appl. Phys. Lett. **109**, 132601 (2016).
[23] G. R. Granstrom, I. Fridman, H.-C. Lei, C. Petrovic, and J. Y. T. Wei, arXiv:1711.00144.
[24] I. I. Mazin, A. A. Golubov, and B. Nadgorny, J. Appl. Phys. **89**, 7576 (2001).
[25] G. J. Strijkers, Y. Ji, F. Y. Yang, C. L. Chien, and J. M. Byers, Phys. Rev. B **63**, 104510 (2001).
[26] R. Vadapoo, S. Krishnan, H. Yilmaz, and C. Marin, Phys. Status Solidi B **248**, 700 (2011).
[27] A. Bera, K. Pal, D. V. S. Muthu, S. Sen, P. Guptasarma, U. V. Waghmare, and A. K. Sood, Phys. Rev. Lett. **110**, 107401 (2013).
[28] I. Efthimiopoulos, J. Zhang, M. Kucway, C. Park, R. C. Ewing, and Y. Wang, Sci. Rep. **3**, 2665 (2013).
[29] W. Li, X.-Y. Wei, J.-X. Zhu, C. S. Ting, and Y. Chen, Phys. Rev. B **89**, 035101 (2014).
[30] I. Efthimiopoulos, C. Buchan, and Y. Wang, Sci. Rep. **6**, 24246 (2016).
[31] G. Cao, H. Liu, J. Liang, L. Cheng, D. Fan, and Z. Zhang, Phys. Rev. B **97**, 075147 (2018).
[32] P. Cheng, C. Song, T. Zhang, Y. Zhang, Y. Wang, J.-F. Jia, J. Wang, Y. Wang, B.-F. Zhu, X. Chen, X. Ma, K. He, L. Wang, X. Dai, Z. Fang, X. Xie, X.-L. Qi, C.-X. Liu, S.-C. Zhang, and Q.-K. Xue, Phys. Rev. Lett. **105**, 076801 (2010).
[33] T. Hanaguri, K. Igarashi, M. Kawamura, H. Takagi, and T. Sasagawa, Phys. Rev. B **82**, 081305(R) (2010).
[34] G. E. Blonder, M. Tinkham, and T. M. Klapwijk, Phys. Rev. B **25**, 4515 (1982).
[35] Y. G. Naidyuk and I. K. Yanson, *Point-Contact Spectroscopy* (Springer, Berlin, 2005).
[36] G. Sheet, S. Mukhopadhyay, and P. Raychaudhuri, Phys. Rev. B **69**, 134507 (2004).
[37] R. J. Soulen, Jr., J. M. Byers, M. S. Osofsky, B. Nadgorny, T. Ambrose, S. F. Cheng, P. R. Broussard, C. T. Tanaka, J. Nowak, J. S. Moodera, A. Barry, and J. M. D. Coey, Science **282**, 85 (1998).
[38] P. P. Kong, F. Sun, L. Y. Xing, J. Zhu, S. J. Zhang, W. M. Li, Q. Q. Liu, X. C. Wang, S. M. Feng, X. H. Yu, J. L. Zhu, R. C. Yu, W. G. Yang, G. Y. Shen, Y. S. Zhao, R. Ahuja, H. K. Mao, and C. Q. Jin, Sci. Rep. **4**, 6679 (2014).
[39] K. Y. Wang, K. W. Edmonds, R. P. Campion, L. X. Zhao, C. T. Foxon, and B. L. Gallagher, Phys. Rev. B **72**, 085201 (2005).
[40] T. McGuire and R. Potter, IEEE Trans. Magn. **11**, 1018 (1975).
[41] T. K. Maji, S. K. Pal, and D. Karmakar, *DAE Solid State Physics Symposium 2017*, AIP Conf. Proc. No. 1942 (AIP, New York, 2018), p. 130053.
[42] H. Wang, H. Liu, C.-Z. Chang, H. Zuo, Y. Zhao, Y. Sun, Z. Xia, K. He, X. Ma, X. C. Xie, Q.-K. Xue, and J. Wang, Sci. Rep. **4**, 5817 (2014).
[43] G. Long, S. Xu, X. Cai, Z. Wu, T. Han, J. Lin, C. Cheng, Y. Cai, X. Wang, and N. Wang, Nanotechnology **29**, 035204 (2018).
[44] F. V. Tikhonenko, A. A. Kozikov, A. K. Savchenko, and R. V. Gorbachev, Phys. Rev. Lett. **103**, 226801 (2009).
[45] G. Kresse and J. Furthmüller, Phys. Rev. B **54**, 11169 (1996).
[46] G. Kresse and D. Joubert, Phys. Rev. B **59**, 1758 (1999).
[47] A. Bansil, H. Lin, and T. Das, Rev. Mod. Phys. **88**, 021004 (2016).